## NOTATION

$\mathbf{r}$, radius vector; x, y, coordinates; $\mathbf{v}$, velocity; $\delta$, Dirac function; f, probability density; $\Phi$, integral distribution function; $\sigma$, mean square deviation; $\nabla$, gradient operator; $\eta$, shear viscosity coefficient; p, pressure; R, tube radius; t, time; Re, Reynolds number; $\gamma$, ratio of Reynolds number to critical value; U, mean flow velocity; $\lambda$, tube resistance coefficient.

## LITERATURE CITED


1. N. N. Bogolyubov, Selected Works [in Russian], Vol. 2, Kiev (1970).
2. I. G. Kirkwood, J. Chem. Phys., 14, No. 3, 180-201 (1946).
3. H. S. Green, Molecular Theory of Fluids, Amsterdam (1952).
4. L. A. Rott, Statistical Theory of Molecular Systems [in Russian], Moscow (1979).
5. L. D. Landau and E. M. Lifshits, Hydrodynamics [in Rusian], Moscow (1986).
6. L. P. Kadanoff, Phys. Today, Dec., 46 (1983).
7. Yu. L. Kilmontovich, Pis'ma Zh. Tekh. Fiz., 10, No. 2, 80-83 (1984).


# DEVELOPMENT AND MOVEMENT OF VORTEX STRUCTURES NEAR THE SURFACE OF A SOLID WALL


I. A. Belov, B. A. Kolovandin, and
N. A. Kudryavtsev



UDC 532.517.2



The dynamics of large-scale vortices near the surface of a plate is modeled on the basis of numerical integration of nonsteady two-dimensional Navier–Stokes equations.


Large-scale vortex structures formed near the surface of a solid wall have a significant influence on momentum transfer and can be used as a means of controlling flow and heat transfer in the boundary layer [1, 2]. In this light, a study we made of the development and movement of vortices near the surface of a solid wall is of more than just theoretical interest. It also makes it possible to at least qualitatively evaluate the effect of vortices on such important flow characteristics as wall friction.

The object of our study was a semiinfinite flat horizontal plate. The vortices were generated by a circular cylinder positioned symmetrically relative to the plate at its front edge. Provision was made for alternate rotation of the cylinder in the clockwise and counterclockwise directions at a specified velocity. The method of study was based on numerical integration of the complete two-dimensional Navier–Stokes equations. Before analyzing the results, we will describe features of the numerical method – which was designed for modeling nonsteady flows. We will also first demonstrate its use in an example involving the solution of a test problem concerning the development of a wake behind an isolated circular cylinder.

1. Numerical Procedure. In constructing the numerical method, we use a difference grid and calculate the velocity components at nodes located a half-step from the nodes where pressure is recorded. Figure 1 shows an element of the grid and a characteristic control volume surrounding the node P. Integration over the control volume reduces the system of equations of continuity and momentum change to the form:

$$I = 0, \tag{1}$$

$$(\partial\Phi/\partial t)\,\mathrm{vol} + F = 0, \tag{2}$$


A. V. Lykov Institute of Heat and Mass Transfer, Academy of Sciences of the Belorussian SSR, Minsk.


Translated from Inzhenerno-Fizicheskii Zhurnal, Vol. 56, No. 6, pp. 900-909, June, 1989. Original article submitted January 28, 1988.




0022-0841/89/5606-0616$12.50

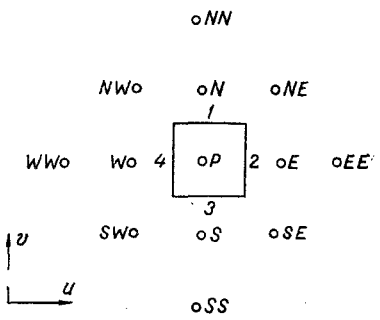


Fig. 1. Element of the grid and characteristic control volume around the node P: 1-4) boundaries of the control volume.

where F is the steady-state part of the impulse equation. This quantity includes the convective and diffusion flows through the boundary of the control volume and the source term.

The difference analog of the continuity equation is exact for the chosen grid model. In the difference approximation of the equations (2) describing the change in momentum, the diffusion flows and source terms are calculated by means of a central-difference approximation. The approximation of the convective flows is most important from the view point of stability and convergence of the numerical process and the accuracy of the results. Our experiment and numerous experiments conducted by other investigators (see [3], for example) show that Leonard's countercurrent quadratic scheme, of third-order accuracy, is optimum in this regard. In accordance with this scheme, when the convective flow ($v_1\Phi_1$) through the first boundary of the control volume is determined (see Fig. 1), the value of $\Phi_1$ is calculated as follows:

$$\Phi_1 = (\Phi_P + \Phi_N)/2 - (\Phi_S - 2\Phi_P + \Phi_N)/8 + (\Phi_W - 2\Phi_P + \Phi_E)/24, \; v_1 > 0; \tag{3}$$

$$\Phi_1 = (\Phi_P + \Phi_N)/2 - (\Phi_P - 2\Phi_N + \Phi_{NN})/8 + (\Phi_{NW} - 2\Phi_N + \Phi_{NE})/24, \; v_1 < 0. \tag{4}$$

Either equations similar to (3-4) or a central difference approximation can be used to determine the value of velocity $v_1$ and the convective flows through the remaining boundaries of the control volume.

As a result of spatial approximation (1-2), we obtain the following system of equations:

$$I_3 + I_4 - I_1 - I_2 = 0; \tag{5}$$

$$[(\partial\Phi/\partial t)\,\mathrm{vol}]_P + a_0\Phi_P + a_1\Phi_N + a_2\Phi_E + a_3\Phi_S + a_4\Phi_W + b_0 = 0, \tag{6}$$

where $I_i$ is the mass flow through the i-th boundary of the control volume; $a_i$ (i = 0-4) are coefficients; $b_0$ is the source term.

In accordance with the well-known SIMPLE procedure, continuity equation (5) is then transformed into the Poisson equation to correct the pressure $\delta p$. The derivation of this equation was described in sufficient detail in previous studies (see [4], for example) and will therefore not be explained here.

It should be noted that the use of expressions of type (3) and (4) in deriving equations of momentum change (6) may lead to a situation whereby the coefficients $a_i$ (i = 1-4) will have different signs and will exceed the coefficient $a_0$ in absolute value. As a result, the numerical process may diverge. To avoid this undesirable effect, we rewrite (3) and (4) as follows:

$$\Phi_1 = \Phi_P/2 + c_1, \; v_1 > 0; \tag{3a}$$

$$\Phi_1 = \Phi_N/2 + c_2, \; v_1 < 0, \tag{4a}$$

where $c_1$ and $c_2$ are found from a comparison of (3) and (3a), as well as (4) and (4a).

Now inserting expressions of the type (3a) and (4a) into (2), we find that the conditions

$0 \leq a_i \leq a_0$ and $\sum_{i=1}^{4} a_i = a_0$. are satisfied. The numerical experiment shows that such "normalization" of the coefficients of Eq. (6) appreciably enhances the stability of the numerical calculation. It should be noted that more complicated but less effective "normalization" procedures were described in [5, 6].

Let us proceed to examine possible schemes for writing the momentum change equation (2) relative to the time layers. In developing the numerical procedure, we studied the following two explicit schemes:

$$\mathrm{vt}\,(\Phi^{N+1} - \Phi^N) + F^N = 0 \tag{7}$$

(Eulerian scheme of first-order accuracy for time);

$$\mathrm{vt}\,(\Phi^{N+1} - \Phi^N) + 1{,}5F^N - 0{,}5F^{N-1} = 0 \tag{8}$$

(Adams–Beshfort scheme of second-order accuracy for time). In (7) and (8), vt = vol/$\Delta$t.

The numerical experiment shows that scheme (7) is dynamically stable for local Curant numbers Cu < 1 but is statically unstable. The latter means that errors accumulate when the computation is continued until the attainment of a nearly steady-state solution. Thus, the numerical process eventually begins to "oscillate." Scheme (8) proved to be absolutely unstable, although there have been instances when it has been used successfully in combination with Arakav's difference scheme (see [7], for example).

Implicit schemes are more efficient. We studied three of them:

$$\mathrm{vt}\,(\Phi^{N+1} - \Phi^N) + F^{N+1} = 0 \tag{9}$$

(scheme of first-order accuracy for time);

$$\mathrm{vt}\,(\Phi^{N+1} - \Phi^N) + 0{,}5\,(F^{N+1} + F^N) = 0 \tag{10}$$

(Crank–Nicolson scheme of second-order accuracy for time);

$$\mathrm{vt}\,(1{,}5\Phi^{N+1} - 2\Phi^N + 0{,}5\Phi^{N-1}) + F^{N+1} = 0 \tag{11}$$

(Peir scheme of second-order accuracy for time).

The most interesting of these schemes is (11), which is superior to the Crank–Nicholson scheme in terms of suppressing nonphysical oscillations of the flow parameters and in regard to the simplicity of devising the algorithm. At the same time, a comparison of scheme (11) and scheme (9) shows that, other conditions being equal, the latter requires fewer time steps to provide acceptable accuracy in modeling nonsteady flow characteristics. Taking this into account, we nonetheless decided to perform all of the below calculations with the use of scheme (11).

It should be pointed out that an iterative procedure is used to ensure that the steady-state part F in Eqs. (9)-(11) is recorded on the (N + 1)-st time layer. The need to qualitatively describe the nonsteady flow characteristics of incompressible fluids nearly precludes the use of noniterative direct methods because they require the introduction of a hypothetical nonsteady term in the continuity equation.

Thus, the computing procedure includes the following operations:

1) assigning the initial conditions $\Phi_0^{N+1}$ for all variables;

2) solving the momentum change equations (11) to determine $u^{N+1}$ and $v^{N+1}$.

3) solving the Poisson equation to correct pressure until convergence is achieved at all nodes of the difference grid (internal iterative cycle);

4) determination of the new pressure field and correction of the velocity components from established values of the pressure correction.

If the momentum change equations have still not converged, then the operations are repeated begining with the second operation (external iterative cycle). Otherwise, we proceed to the next time layer and perform all operations again, beginning with the first.

It is evident from the foregoing that the efficiency of the numerical procedure for calculating nonsteady flows is determined mainly by the sum of iterations in the internal and external iteration cycles performed at the N time steps required to obtain the steady-state solution. From this viewpoint, the choice of the initial values of all variables $\phi^{N+1}$ and the procedure used to solve the difference equations are particularly important.

The numerical experiment shows that it is most efficient to determine the initial (linearized) values of the velocity components by means of the simple relations

$$u_0^{N+1} = u^N + \Delta u^N; \quad v_0^{N+1} = v^N + \Delta v^N, \tag{12}$$

where $\Delta u^N = u^N - u^{N-1}$; $\Delta v^N = v^N - v^{N-1}$.

At the same time, it is inexpedient to perform a linearization of the type (12) for the pressure field, since nonphysical oscillations of the flow parameters take place and there is an increase in the total number of iterations in the internal and external cycles. Thus, for pressure take $p_0^{N+1} = p^N$.

Now let us examine a method of solving difference equations which is based on the transformation of a five-diagonal matrix (FDMA). All of the difference equations can be represented as follows after normalization of their coefficients (see Fig. 1)

$$\Phi_P = a_N\Phi_N + a_E\Phi_E + a_S\Phi_S + a_W\Phi_W + b, \tag{13}$$

where $\Phi \equiv u$, v, or $\delta p$; b is the source term; $a_K$(K = N, E, S, W) are coefficients subject to the conditions $0 \leq a_K \leq 1$ and $\sum_K a_K \leqslant 1$ .

We represent Eq. (13) in the form

$$\Phi_P = A_N\Phi_N + A_E\Phi_E + B. \tag{14}$$

Then we can write:

$$\Phi_S = (A_N)_S\Phi_P + (A_E)_S\Phi_{SE} + B_S; \tag{15}$$

$$\Phi_W = (A_N)_W\Phi_{NW} + (A_E)_W\Phi_P + B_W. \tag{16}$$

Inserting (15) and (16) into (13) and comparing the result with (14), we obtain:

$$A_N = a_N/D; \; A_E = a_E/D; \; B = \{b + a_S[(A_E)_S\Phi_{SE} + B_S] + a_W[(A_N)_W\Phi_{NW} + B_W]\}/D, \tag{17}$$

where $D = 1 - a_3(A_N)_S - a_4(A_E)_W$.

The procedure for solving Eq. (13) involves initially determining the coefficients $A_N$, $A_E$, and B by means of (17). Here, the grid nodes should be circumvented "from left to right" and "from top to bottom" (forward trial run). We then calculate the variable $\Phi$ from Eq. (14) with reverse circumvention of the nodes (reverse trial run). In performing these operations, we are essentially dividing the initial five-diagonal matrix (13) into upper (14) and lower (17) triangular matrices.

It should be noted that Eq. (14) can be written in the form

$$\Phi_P^{m+1} = A_N^m\Phi_N^{m+1} + A_E^m\Phi_E^{m+1} + B^m \tag{14a}$$

or

$$\Phi_P^{m+1} = A_N^m\Phi_N^m + A_E^m\Phi_E^m + B^m. \tag{14b}$$

The numerical experiment shows that in the solution of the Poisson equation for the pressure correction ($\Phi = \delta p$), both forms lead to conditional stability of the internal iteration cycle. However, convergence is faster when form (14a) is used. At the same time, in solving the momentum change equations ($\phi$ = u or v), only the use of (14b) ensures good stability of the external iteration cycle and its satisfactorily rapid convergence. The use of (14a) in this case leads to oscilaltions of the velocity components that are hard to extinguish even by introducing under-relaxation.

The numerical studies established that the FDMA method provides for more rapid convergence of the external and internal iteration cycles compared to the method of inversion

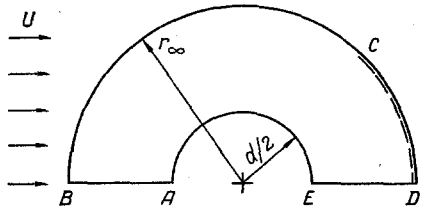


Fig. 2. Theoretical region: d) diameter of cylinder; $r_\infty$) external boundary; U, velocity of the undisturbed flow.

of a tridiagonal matrix. Moreover, the FDMA method is sufficiently simple to realize and permits the inclusion of any relaxation parameters.

2. Check of the Numerical Procedure. The efficiency of the above-described procedure was checked by calculating the development of a circulation zone formed in the wake of an isolated circular cylinder of diameter d. The cylinder was suddenly brought into motion with a constant velocity U. We chose a value of 40 for the Reynolds number determined on the basis of these parameters. The time t is normalized with respect to the ratio d/U. The value t = 0 corresponds to the beginning of the motion of the cylinder.

The problem is solved in a polar coordinate system (r, $\vartheta$). Figure 2 shows the theoretical region. In accordance with the inversion principle, we assign conditions corresponding to undisturbed flow on the external boundary of the theoretical region BC. We use "mild" conditions for the velocity components on the rear part of the external boundary CD. Flow symmetry conditions are established for the surfaces AB and DE. Finally, conditions of adhesion of the fluid are satisfied on the surface of the cylinder AE, while friction is calculated on the basis of cubic interpolation of the boundary profile of tangential velocity.

The theoretical polar grid is characterized by the following parameters: step of the grid in the tangential direction $h = \pi/30$; external boundary located the distance $r_\infty = 158d$ from the center of the cylinder; total number of grid nodes $32 \times 56$. We also note that we introduce the under-relaxation coefficient 0.6 in solving the equation of momentum change (14b) and the over-relaxation coefficient 1.3 in the solution of the Poisson equation for the pressure correction (14a). The solution of the initial equations in the external and internal iteration cycles converges with an accuracy not exceeding $10^{-4}$. However, the number of iterations in the external cycle is limited from below to two in order to ensure that the character of the solution of the momentum equations is strictly implicit.

The problem of the development of a circulation zone formed in the wake of an isolated circular cylinder was solved with the choice of time steps $\Delta t = 0.05$, 0.1, 0.5, and 2.0. Analysis of the theoretical data shows that the results obtained with $\Delta t = 0.05$ and 0.1 agree and are satisfactory in terms of accuracy. The use of larger time steps ($\Delta t = 0.5$ and 2.0) distorts the process of establishment of the flow characteristics. As confirmation of this, Tables 1 and 2 show the results of calculation of the length of the circulation zone and the angle of flow separation on the cylinder surface at different moments of time (both quantities were reckoned from the rear stagnation point of the cylinder). This information is compared in the table with experimental data from [8] and numerical results from [9]. It should be noted that in [9] the initial equations were written in the variables of the stream function – vorticity, with the use of the time step $\Delta t = 0.04$. Also, the author here used a polar grid with the step $h = \pi/30$ in the tangential direction; the initial equations were approximated by means of a central-difference scheme; the curl transport equation was solved by using the implicit method of variable directions, while the Poisson equation for the stream function was solved by the method of successive over-relaxation.

Figure 3 shows the process of establishment of the solution in the form of a sequence of flow patterns. Here, $\Delta t = 0.1$, which ensures satisfactory accuracy in the modeling of the nonsteady process of wake development. One feature of the solution is the sharp initial increase in the intensity of the circulation zone up to the time t = 3.2 and its subsequent gradual reduction.

In conclusion, we note that the numerical procedure developed here makes it possible to obtain the steady-state solution with sufficient speed if there is no need to accurately

TABLE 1. Change over Time in the Length of the Circulation Zone Developing in the Wake of an Isolated Circular Cylinder (Re = 40)

| Source | $t$ | | | | | | | | |
|---|---|---|---|---|---|---|---|---|---|
| | 1 | 2 | 3 | 4 | 5 | 6 | 8 | 10 | 12 |
| [8], experiment | 0,36 | 0,74 | 1,11 | 1,41 | 1,65 | 1,85 | 2,05 | 2,18 | 2,19 |
| [9], calculation | 0,36 | 0,85 | 1,30 | 1,63 | 1,85 | 2,20 | 2,45 | 2,54 | 2,54 |
| Pres.st. $\Delta t = 0,1$ | 0,30 | 0,74 | 1,10 | 1,39 | 1,62 | 1,80 | 2,03 | 2,12 | 2,15 |
| Pres.st. $\Delta t = 0,5$ | 0,12 | 0,57 | 0,95 | 1,28 | 1,56 | 1,78 | 2,07 | 2,15 | 2,15 |
| Pres.st. $\Delta t = 2,0$ | — | 0 | — | 0,73 | — | 1,30 | 1,76 | 2,12 | 2,37 |

TABLE 2. Change over Time in the Angle of Flow Separation on the Surface of an Isolated Circular Cylinder (Re = 40)

| Source | $t$ | | | | | | | | |
|---|---|---|---|---|---|---|---|---|---|
| | 1 | 2 | 3 | 4 | 5 | 6 | 8 | 10 | 12 |
| [8], experiment | 41,2 | 46,5 | 49,3 | 51,0 | 52,1 | 52,7 | 53,1 | 53,4 | 53,4 |
| [9], calculation | 49,0 | 51,5 | 52,2 | 52,7 | 53,0 | 53,3 | 53,5 | 53,7 | 53,7 |
| Pres.st. $\Delta t = 0,1$ | 48,7 | 52,0 | 52,7 | 53,1 | 53,4 | 53,6 | 53,9 | 54,0 | 54,1 |
| Pres.st. $\Delta = 0,5$ | 47,5 | 54,0 | 52,8 | 52,7 | 53,2 | 53,5 | 53,8 | 54,0 | 54,1 |
| Pres.st. $\Delta t = 2,0$ | — | 0 | — | 59,0 | — | 55,4 | 53,6 | 53,6 | 54,0 |

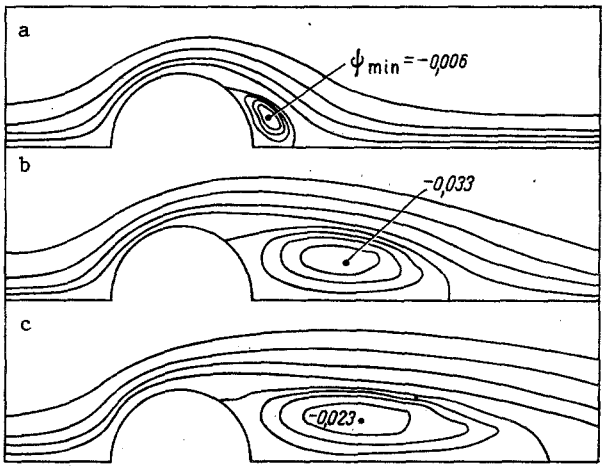


Fig. 3. Flow patterns around an isolated circular cylinder in the form of lines of constant values of the steam function $\psi = 0.75\ \psi_{min}$; 0.5; 0.25; 0; 0.02; 0.04; 0.1 and 0.2; a) t = 1; b) 4; c) 10.

describe the process of estabishing this solution. In particular, with the choice of times steps $\Delta t$ = 0.1 and 2.0, 61 and 21 min of processor time are needed on an ES-1050 computer to obtain a completely steady (t = 20) solution to the problem in question. Evidence of the accuracy of the steady-state solution comes from its good agreement with the results of numerical studies surveyed in [8].

3. Development and Movement of Vortex Structures Near the Surface of a Semiinfinite Plate. We will examine nonsteady flow about a circular cylinder in the case where a plate DE (see Fig. 2) is located in the wake of the cylinder in the plane of symmetry. To retain the features of the formulation and solution of the test problem of flow abut an isolated cylinder, we used the same theoretical region as previously. Here, conditions of continuation of the solution are assigned on the boundary AB, while conditions of adhesion of the fluid are assigned on the boudnary DE. The conditions remain the same as before on all of the other boundaries.

The goal in solving the present problem is to study the possibility of reducing friction resistance on the wall DE by moving vortices formed in the cylinder wake along the wall.

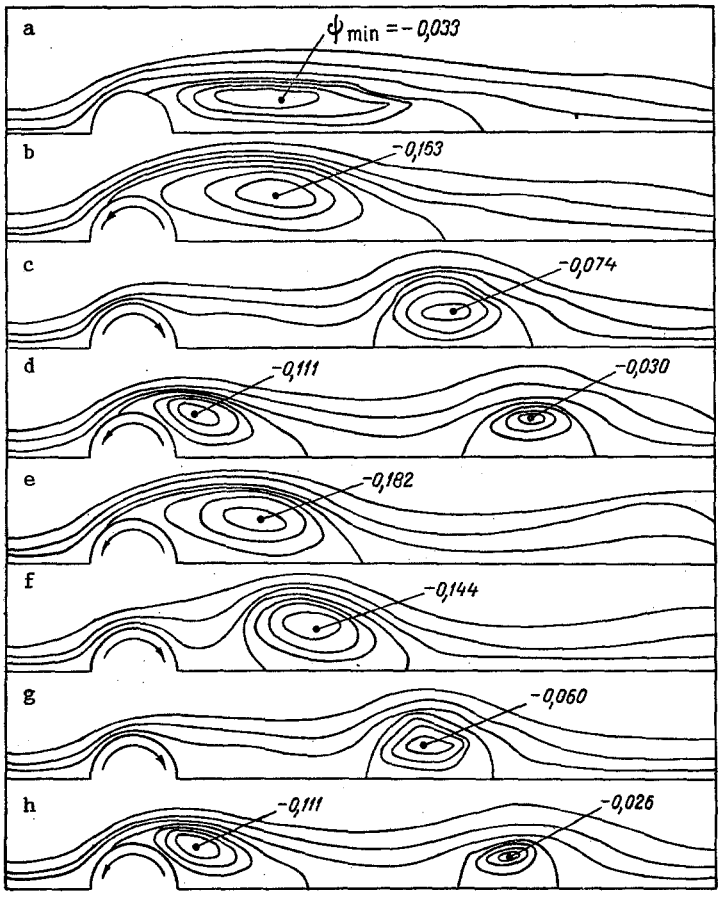


Fig. 4. Development and movement of vortex structures near the surface of a seminfinite plate. Here, the streamlines $\psi = 0.75\ \psi_{min}$; 0.5; 0.25; 0; 0.04; 0.1 and 0.2; a) t = 0; b) 5; c) 10; d) 12; e) 15; f) 17; g) 20; h) 22.

The characteristic Reynolds number, determined from the velocity of the undisturbed flow and the diameter of the cylinder, was taken equal to 100.

Separation of the vortices from the cylinder surface was accomplished by rotating the cylinder at a specified velocity in the clockwise direction. At the same time, to ensure the subsequent drift of each vortex along the plate over a large distance (to increase its lifetime until complete dissipation), we also arranged for the cylinder to rotate in the opposite direction (counterclockwise). The mechanism of acceleration and deceleration of a flow by a moving wall was described in [10] using the example of the development of a Kármán vortex street in the wake of a rotating cylinder. The calculation was performed with a cylinder-surface velocity $u_w = \pm 0.5$ (in fractions of the velocity U), respectively, for the motion of the cylinder in the clockwise and counterclockwise directions. We took $\Delta T = 5$ as the time interval during which the cylinder rotated in one direction or the other. The calculations were performed with a time step $\Delta t = 0.2$ up to the moment t = 22.

Let the initial moment of time t = 0 correspond to flow about a stationary cylinder. The flow pattern in this case is shown in Fig. 4a. It is evident that the vortex in the nearby wake behind the cylinder is of low intensity. Rotation of the cylinder in the counterclockwise direction during the chosen time interval $\Delta T = 5$ increases the intensity of the vortex (see Fig. 4b). The direction of cylinder rotation was changed at the moment t = 5, which caused the vortex to separate and drift along the plate (see Fig. 4c for t = 10). A change in the direction of cylinder rotation at the moment t = 10 led to the formation of a new vortex adjacent to the cylinder; here, the previously-formed vortex continued to move downflow along the plate (see Fig. 4d for t = 12). A gradual decay of the shed vortex and an increase in the intensity of the attached vortex can be seen in Fig. 4e at t = 15. The flow patterns are repeated at subsequent moments of time (see Fig. 4f-h) for t = 17, 20, and 22).

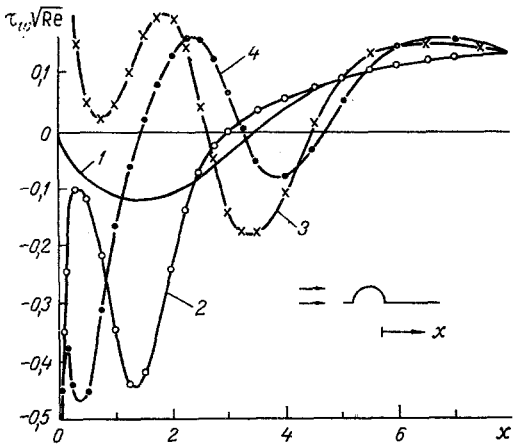


Fig. 5. Distribution of friction $\tau_w$ on the plate 1) t = 0; 2) 5; 3) 10; 4) 12.

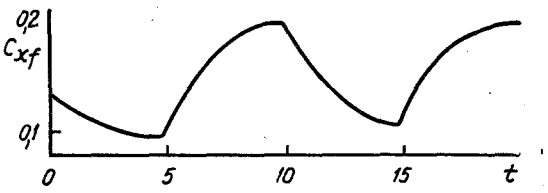


Fig. 6. Dependence of the drag coefficient of the plate ($\Delta x$ = 8d) on time.

Figures 5 and 6 show some quanitative results of calculation of the flow being examined. Figure 5 shows the relation for friction on the pate $\tau_w(x)$ at fixed moments of time corresponding to the flow patterns in Fig. 4a-d. Figure 6 shows the time dependence of the drag coefficient $C_{xf}$ of the plate DE ($C_{xf}$ was calculated for the surface of a plate of the length 8d). It should benoted that in the case of nonseparated flow about a semiinfinite plate, friction is calculated from the formula $\tau_w = 0.664/Re_x^{1/2}$, where $Re_x$ is the Reynolds number determined from the distance from the leading edge of the plate. Integration of the last relation in the range of x from 0 to 8d yields a drag coefficient $C_{xf} = 0.376$.

It should be pointed out that the calculated results presented here do not fully reflect the actual pattern of flow, since the relatively coarse polar grid used in the calculation causes rapid nonphysical dissipation of the vortices at large distances from the cylinder due to the mechanism of numerical diffusion. In particular, this causes the absolute values of the negative flow corresponding to the attached vortex (see curve 2 in Fig. 5) to decrease sharply with increasing distance between the vortex and the cylindder (curves 3 and 4 in Fig. 5). At the same time, analysis of the experimental data [11] shows that each individual vortex moving near the wall is a fairly complex structure capable of creating its own velocity field for a short period of time after it is acted upon by the local perturbation. An example of this point out in [11] is the conservation of the Kármán street in the wake of an isolated cylidner even when a plate dividing this street is introduced into the wake region in the diameter plane of the cylinder. It should also be noted that a Kármán street is also seen at a distance x/d from the cylinder of about 300 when Re = 90 [12].

The method chosen in the present study for organizing vortex structures near the surface of a wall cannot be considered optimal if it is necessary to minimize the resistance of the wall while also minimizing the losses due to the resistance of the vortex generator itself (in the present case, the circular cylinder). In fact, the continued presence of the circular cylinder in the flow leads to situation whereby the total resistance of the cylinder and wall turns out to be quite high. It can be reduced significantly both by selecting more efficient (in terms of resistance) forms of vortex generator and by inserting the latter into the flow periodically, during limited time intervals (see [13] as an example).

## NOTATION

$\Phi$, variable; u, v, velocity components; p, pressure; $\delta p$, pressure correction; $\psi$, stream function; t, time; $\Delta t$, time step; $\Delta T$, time interval during which cylinder is rotated in one direction; I, mass source of flow; vol, control volume; Re, Reynolds number; (r, v), polar coordinate system; x, longitudinal coordinate; h, step of grid; A, B, C, $a$, b, c, coefficients; $\tau_w$, friction; $C_{xf}$, drag coefficient. Indices: i, number of boundary of control volume (i = 1-4); P, W, S, ..., n; N, number of time step; m, number of iteration step; w, wall; $\infty$, external boundary of theoretical region.

## LITERATURE CITED


1. I. A. Belov, Interaction of Nonequilibrium Flows with Barriers [in Russian], Leningrad (1983).
2. R. I. Soloukhin, B. A. Kolovandin, B. I. Puris, et al., Turbulent Transport Processes [in Russian], Minsk (1985), pp. 3-15.
3. M. A. Leschziner, Comp. Meth. Appl. Mech. Eng., 23, No. 3, 293-312 (1980).
4. S. Patankar, Numerical Methods of Solving Problems of Fluid Dynamics and Heat Transfer [in Russian], Moscow (1984).
5. T. Han, J. A. C. Humphrey, and B. E. Launder, Comp. Meth. Appl. Mech. Eng., 29, No. 1, 81-95 (1981).
6. A. Pollard and A. L.-W. Siu, Comp. Meth. Appl. Mech. Eng., 35, No. 3, 293-313 (1982).
7. I. A. Belov and N. A. Kudryavtsev, Inzh.-Fiz. Zh., 41, No. 2, 310-317 (1981).
8. M. Coutanceau and R. Bouard, J. Fluid Mech., 79, Pt. 2, 257-272 (1977).
9. J. S. Son and T. J. Hanratty, J. Fluid. Mech., 35, Pt. 2, 369-386 (1969).
10. L. E. Ericsson, AIAA J., 18, No. 8, 935-944 (1980).
11. R. Ville, Problems in Mechanics [in Russian], Moscow, 226-238 (1963).
12. M. M. Zdravkovich, J. Fluid Mech., 37, Pt. 3, 491-496 (1969).
13. H. Viets, M. Piatt, and M. Ball, AIAA Paper, No. 0256, 1-9 (1981).